Monthly Notices
of the
ROYAL ASTRONOMICAL SOCIETY

MNRAS **441,** 2744–2753 (2014) doi:10.1093/mnras/stu760

Looking for activity cycles in late-type *Kepler* stars using time–frequency analysis

K. Vida,★ K. Oláh and R. Szabó

Research Centre for Astronomy and Earth Sciences, Hungarian Academy of Sciences, H-1121 Budapest, Hungary

Accepted 2014 April 15. Received 2014 April 12; in original form 2013 October 4

ABSTRACT

We analyse light curves covering four years of 39 fast-rotating ($P_{\rm rot} \lesssim 1$ d) late-type active stars from the *Kepler* data base. Using time–frequency analysis (short-term Fourier transform), we find hints for activity cycles of 300–900 d at nine targets from the changing typical latitude of the starspots, which with the differential rotation of the stellar surface change the observed rotation period over the activity cycle. We also give a lowest estimation for the shear parameter of the differential rotation, which is ≈0.001 for the cycling targets. These results populate the less studied, short-period end of the rotation–cycle length relation.

Key words: stars: activity – stars: late-type – stars: magnetic field.

1 INTRODUCTION

The 11 year and other, longer activity cycles of the Sun have been known for a long time, and similar multiple cycles have been recovered for many active stars (see Oláh et al. 2009 and references therein). Systematic studies of stellar cycles began with the Ca H&K survey at Mount Wilson (Wilson 1968), and with the advent of the automated photometric telescopes (see e.g. Strassmeier et al. 1997). To study this phenomenon, long-term observations are needed, as the typical time-scales of the cycles range from a few years to decades. A correlation has been found between the rotation period and the length of the activity cycle, as shown first by Baliunas et al. (1996) and recently by Oláh & Strassmeier (2002), namely that on faster rotating stars the activity cycles tend to be shorter.

Planned and currently developing long-term all-sky surveys, such as the Large Synoptic Survey Telescope (see Ivezić et al. 2008), the PASS (Deeg et al. 2004) and the Fly's Eye Camera System (Pál et al. 2013), may give a huge thrust to this field, provided they run for many years, even decades, since not only selected objects (which may contain no suitable targets and miss interesting ones) but the whole sky will be monitored.

At present though, the best option for monitoring stars is the *Kepler* space telescope, providing an almost continuous data set of unprecedented precision from about 160 000 targets, among them thousands of active stars. The already recovered stellar cycles range from years to decades, while the *Kepler* space telescope operated only for four years. Vida, Kriskovics & Oláh (2013) analysed long-term photometric measurements of ultrafast-rotating ($P_{\rm rot} \approx 0.5$ d) M dwarfs, and found activity cycles on three stars with cycle lengths between 300 and 500 d, which is already within the reach of *Kepler*.

Magnetic activity, rotation and differential rotation of *Kepler* stars are in the focus of research lately (see e.g. Karoff et al. 2013; Mathur et al. 2014; Walkowicz & Basri 2013). McQuillan, Aigrain & Mazeh (2013a) developed a robust method using an autocorrelation function to determine rotation periods from light curves and studied more than 2400 stars. The method was applied later by McQuillan, Mazeh & Aigrain (2013) to *Kepler* Objects of Interest to study exoplanet-hosting systems. Nielsen et al. (2013) used Lomb–Scargle periodograms to search for rotation periods in *Kepler* targets; the authors analysed 12 000 F-, G- and K-type stars. The same method was applied by Reinhold, Reiners & Basri (2013) to study more than 40 000 active *Kepler* stars; they also made an effort to estimate the values of the differential rotation shear.

Working with *Kepler* data has its own drawbacks. There are instrumental trends during each observing quarter, and shorter term instrumental glitches are also present on a time-scale of a few days. Although there are attempts to correct these trends (and not just remove them automatically), the possibility of having a homogeneous light curve ranging many observing quarters seems really hard to achieve. Hence, the information on long-term cycles, which can be basically seen by naked eye on a persistently observed earth-borne light curve from photometry, is lost in the *Kepler* data.

Or is it? Are there other properties of the activity cycles that can help us to trace them? One realization of the 11 yr cycle on the Sun is the butterfly diagram, i.e. the phenomenon that the sunspots tend to appear on higher latitudes at the beginning of the cycle and closer to the equator at its end. There have been attempts to recover this migration of typical spot latitudes on other active stars (see e.g. Berdyugina & Henry 2007). Lately, Katsova et al. (2010) used wavelet analysis of Ca H&K data from the Mount Wilson survey to determine the variations in the rotation period of active stars, and studied similar cyclic variation of the solar corona, from a 'Sun as a star' approach.

★ E-mail: vidakris@konkoly.hu

Recent theoretical dynamo models are able to describe the butterfly diagram reliably for different kinds of active stars. Fig. 10 in Işık, Schmitt & Schüssler (2011) shows the modelled spot distribution of a fast-rotating ($P_{\rm rot} = 2$ d) K0V star during its activity cycles. According to the model, the well-known shape of the butterfly diagram changes substantially as a result of the fast rotation. The flux tubes – even if started from a similar configuration as the Sun – emerging from the tachocline reach the photosphere at much higher latitudes than on the Sun. Unfortunately, in this fast-rotating, late-type stellar case, the latitude distribution also changes: the spots appear in a much thinner latitude stripe (between about 35° and 45°) in the model, in contrast with observed solar case (between about 0° and 40°). Compared to the Sun, a much smaller modulation of the emerging latitudes is still found in the model during the activity cycle, but most of the emerging spots appear almost at the same latitude. Thus, the butterfly diagram in this case resembles much less to a butterfly, as the effect is almost washed away by the overlapping 'butterfly wings' (cf. fig. 9 in Işık et al. 2011).

With a strong enough differential rotation however, there might be a difference in the rotational period even in the case of the small latitudinal migration of the fast-rotating active dwarf stars that is still large enough to be detected by high-precision long-term photometry with good time coverage, such as data of the *Kepler* survey. The signal we have to look for is a small change in the typical latitude of spot emergence of a differentially rotating stellar surface, which would result in a very small quasi-periodic change in the photometric rotational period during an activity cycle. Long-term change of the rotational periods can be revealed by time series period searching methods. Such an effect has already been detected on the long-period giant active star CZ CVn by Strassmeier et al. (2011).

In this paper, we look for cycles on fast-rotating active dwarf stars through the systematic changes of their observed rotational periods due to differential rotation.

2 TARGET SELECTION

Vida et al. (2013) found activity cycles with periods of the order of 1 yr on fast-rotating late-type stars; we based the target selection on these objects. As first selection, we looked for dwarfs (with $\log g \approx 4.5$) cooler than 4500 K in the Kepler Input Catalogue (KIC),[1] which resulted in 8826 objects. Then we analysed the light curves of these objects for one (Q1) quarter[2] of data using an automated method. This was done by applying discrete Fourier transformation on the light curves using the one-dimensional option of TIFRAN (Time–Frequency Analysis) package[3] (Csubry & Kolláth 2004). The highest peak of the resulting spectrum was then assigned as rotational period of the given target (for an example of these spectra, see the top plot of Fig. 1). Note that the highest peak in the Fourier spectrum does not necessarily correspond to the rotation period (e.g. if two active regions are separated by ≈180°, the double frequency can be stronger), but this method can be useful to select some suitable candidates from a large sample for more thorough inspection. From the result of this automated Fourier analysis, we selected 113 objects with short period ($P_{\rm rot} \lesssim 1$ d), and then narrowed the list to single stars, where the light curve obviously indicated spottedness,

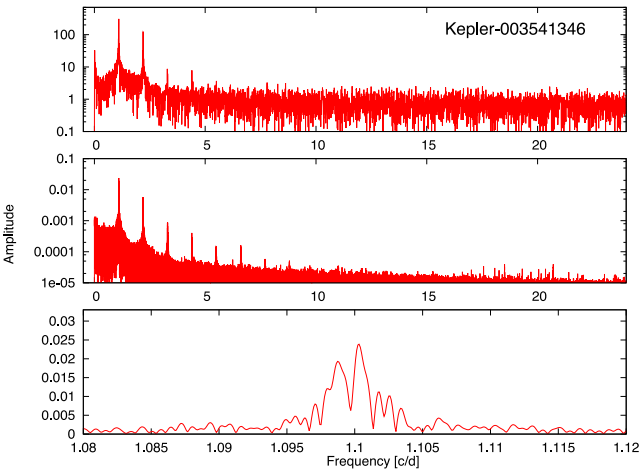

Figure 1. An example Fourier spectrum of Kepler-003541346. The spectrum on the top was made using unprocessed instrumental data (in flux units) only from Q1, used for the automated period search. The middle plot uses all available data, cleaned and interpolated, as used for further analysis (in magnitude units). The bottom plot shows the area of the rotation frequency; the multiple peaks indicate active regions with different rotation periods as a result of differential rotation. The upper two plots are in a logarithmic scale.

i.e. the light variation showed continuous changes in time, resulting in 39 targets. The formal error of the determined rotation periods can be estimated by using the frequency value at 90 per cent of the spectral window. This corresponds to 10 per cent precision (see Oláh, Jurcsik & Strassmeier 2003). This is 0.0025[1/d] in frequency, and is basically the same for all stars, as the properties of the data are the same. This formal error is however not quite meaningful, as the rotation period itself is changing in time.

For these objects, all the publicly available long-cadence data were downloaded from the *Kepler* data base (until Q16). For our analysis, we used PDCSAP_FLUX data created by the regular PDC-MAP algorithm, processed by pipeline version 9.0 (for more details, see Kepler Data Release Notes[4]). We used light curves with version number 5.0, where the timing error of the *Kepler* light curves is already corrected. For further investigation, the light curves were transformed from instrumental flux to magnitude scale (the small amplitude of the light curves causes negligible difference in the Fourier frequencies resulting from the difference of the magnitude/intensity scale). We fit each observing quarter by a third-order polynomial, which was removed from the original light curves, giving a homogeneous light curve varying around zero magnitude. This helped us to get rid of the long-term instrumental changes. These long-term trends might affect the Fourier analysis, although the changes on this time-scale should be independent in Fourier space from the signals of the order of the rotation period.

As a sanity check we examined the contamination values provided by the MAST catalogue[5] for those targets that indicated possible activity cycles (see Section 4). In each case, we found a non-zero value: the numbers range from a few per cent up to 25–30 per cent (depending on the observing quarter, see Table 1). The percentage refers to an estimate of the flux that comes from the contamination, i.e. close-by stars contributing to the sum of flux in the assigned *Kepler* aperture mask.

[1] http://archive.stsci.edu/kepler/kic.html, see Brown et al. (2011b)
[2] For the definition and dates of the *Kepler* observing quarters (marked as e.g. Q1), see http://archive.stsci.edu/mast_faq.php?mission=KEPLER#35
[3] http://www.konkoly.hu/tifran/
[4] http://keplerscience.arc.nasa.gov/Documentation.shtml
[5] http://archive.stsci.edu/kepler

Table 1. Basic data on the interesting *Kepler* targets according to the Kepler Input Catalogue. Contamination values show minimum/maximum flux contamination from other stars; † shows targets, where light contamination change is higher than 8 per cent. The periods were found using automated discrete Fourier transformation. The last two columns show our estimate for cycle lengths and the percentage of the period change. L means a long-term trend in the plot. Kepler-10063343 is shown as an example, where no variations in the rotation period were found. Detected periods for targets marked with ‡ are more uncertain, see Section 5 for details. The last three lines show the objects from Vida et al. (2013), on whose the target selection of the current study was based. The α parameter in the last column gives our lowest estimate of the differential rotation shear, see discussion in Section 6.

KIC ID	Kepler mag.	Contamination (%) min.	max.	$T_{\rm eff}$	log g	$P_{\rm rot}$ (d)	$P_{\rm cyc}$ (d)	$\Delta P_{\rm rot}$ (%)	$\alpha_{\rm min}$
03541346	15.379	11.4	16.4	4194	4.503	0.9082	330 (50)	0.25	0.0027
04819564	14.672	3.7	7.8	4125	4.511	0.3808	530 (150)	0.06	0.0016
04953358	15.487	14.1	26.5†	3843	4.608	0.6490	600 (200)/L‡	0.05	0.0008
05791720	14.067	2.2	6.0	3533	4.132	0.7651	320 (60)	0.12	0.0016
06675318	15.242	3.1	9.3	4206	4.465	0.5777	370 (60)	0.09	0.0016
07592990	15.788	18.6	32.4†	4004	4.632	0.4421	500 (80)‡	0.05	0.0012
08314902	15.745	4.9	13.4†	4176	4.480	0.8135	330 (50)/610 (100)‡	0.08	0.0010
10515986	15.592	9.7	18.1†	3668	4.297	0.7462	350 (50)‡	0.22	0.0030
11087527	15.603	6.5	9.1	4303	4.556	0.4110	310 (70)/650 (300)	0.05	0.0012
12365719	15.843	7.6	19.4†	3735	4.473	0.8501	Inconclusive	–	–
10063343	13.164			3976	4.433	0.3326	–	0.03	–
EY Dra						0.4587	350		
V405 And						0.4650	300		
GSC 3377-0296						0.4225	530		

These relatively high numbers motivated a more thorough check, namely we downloaded the target pixel files for our 10 targets and checked whether the rotation signal comes from the target or a close neighbour. To do this, we choose the most contaminated quarters for each stars. We found that in all cases the rotational variation originates from the target star, and within *Kepler*'s resolution no additional variation is found from off-target pixels. We have to mention that although a long-term contaminating variation from nearby stars (that might alter the amplitude of the rotational variation) would be much harder to exclude this way, our target stars are much more brighter than their surrounding pixels, so a large amplitude variation that would compromise the conclusions of this paper can be safely excluded in all cases.

3 METHOD

The data were examined using various approaches of the TIFRAN package to select the promising candidates. The light curves of the selected targets were cleaned from the extremely outlying points, caused by flares. According to Kolláth & Oláh (2009), Fourier signals of ill-sampled data are much harder to recover; thus, the light curves were interpolated to the *Kepler* sampling to cover the gaps in the observations. We used linear interpolation to fill the gaps in the data sets, which results in straight lines in the missing parts, but this does not alter the main results. We used a short-term Fourier transform (STFT) in this study and report the results in Fig. 2; for a description of this and other, different approaches see Kolláth & Oláh (2009).

An STFT plot might look incomprehensible at first sight, but it is a most helpful tool for time–frequency analysis. The STFT method applies a Gaussian window on the light curve, and by moving this window a sequence of Fourier spectra is obtained. The vertical changes in these plots indicate a shift in a peak in the Fourier spectrum in time; the z-axis (colour code) shows the amplitude of the signal. An α parameter (see equation 2 in Kolláth & Oláh 2009) regulates the width of the Gaussian window, i.e. the balance between temporal and frequency resolution. This was fine-tuned for each cycling target in Fig. 2 to recognize the changes easily.

Strong light contamination from other sources in the *Kepler* aperture can decrease the amplitude of the light curves. This effect can decrease the precision of the frequency determination. Thus, such contamination could make the determination of the cycle lengths harder (even more if it changes through observing quarters), but it does not change the frequency itself. This effect might be seen in Table 1: targets with higher light contamination change (marked with †) have less confidently determined activity cycles (marked with ‡). The tests on artificial data however showed that the method we used to determine the cycle lengths is not very sensitive to amplitude changes (see Appendix A).

4 RESULTS

In 9 of the 39 promising targets, we found signs of cyclic or long-term modulations in the rotation period, which we interpret as a manifestation of stellar activity cycles. The basic parameters of these targets are summarized in Table 1. The light curves and the time–frequency analysis of these objects are plotted in Fig. 2. The last plot in Fig. 2 is used as comparison; for that star, which otherwise is similar to the studied objects, no such modulation was found.

We know from the Sun, and also from long-term photometric analysis of active stars (Oláh et al. 2009), that activity cycles are not strictly regular phenomena. Multiple cycles exist, and also the length of the cycles changes in time. Therefore, one should be cautious when trying to fit exact parameters to quantify the results; often a mere visual inspection can be the most effective, especially, since the data sets cover only a few cycles.

However, as an experiment for a quantitative description, we analysed the STFT of the light curves using a method based on

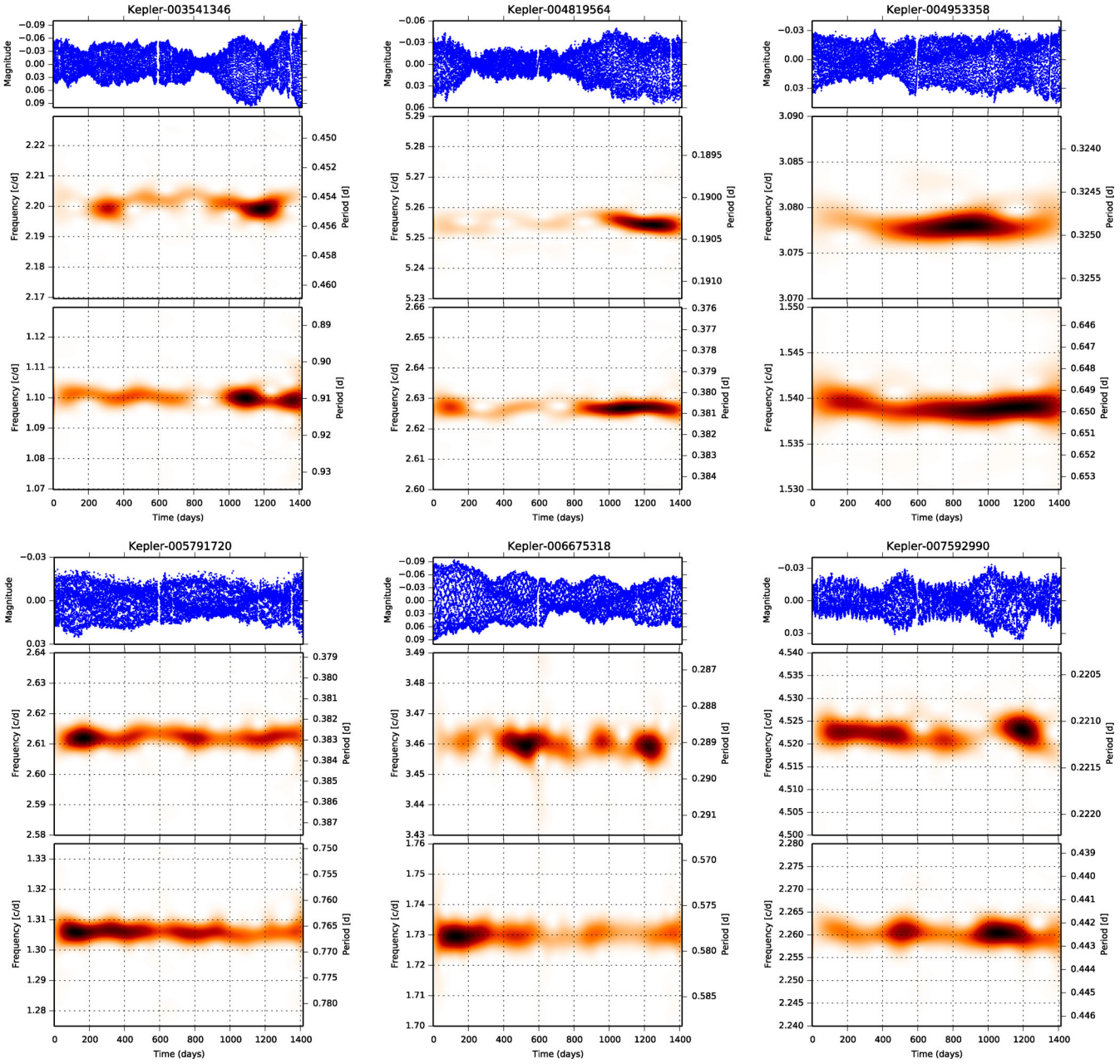

Figure 2. Cleaned and interpolated light curves (top panels) and their STFTs (middle and bottom panels) for the *Kepler* targets where sign of activity cycles was found. The middle and bottom panels show the STFTs at the double of the rotation frequency and at the rotation frequency, respectively. Kepler-10063343 is shown as a comparison, where no change in the rotation frequency was found.

the Fourier transformation of the STFT maxima around the rotation frequency: basically we were looking for detectable periodic signals in the STFT itself (see Fig. 3). This method, however, should be used with much caution and sanity, as signals with periods of the order of the length of the data sets are often present and are not necessarily real. Also, if light-curve amplitudes change very much from cycle to cycle, the recovery of cycle length by this correlation method can get difficult. A clear estimate of the cycle time-scale directly from the STFT helps to find the real signal in this Fourier spectrum (as human brain is much better in pattern recognition than any software). The result of this analysis is summarized in Table 1. This method can be also used to estimate the uncertainties of the cycle lengths. Using the frequency difference between the maximum and half-maximum of the peak in this Fourier transform as an error gives 50–100 d as the typical uncertainty of the cycle lengths.

We analysed each target using discrete Fourier transformation with MUFRAN (Multiple Frequency Analysis; Kolláth 1990) as well, examining 30–200-d-long subsets of the light curve. In this way the stability of the rotational periods of the active regions present in that segment could be checked. As starspots appear on the surface at different latitudes, multiple peaks appear in the Fourier spectrum, thanks to the differential rotating surface (see the bottom panel of Fig. 1). In the case of continuous period change due to differential rotation, the length of the light-curve segment shows that in how long data set the double or multiple peaks appear in the Fourier

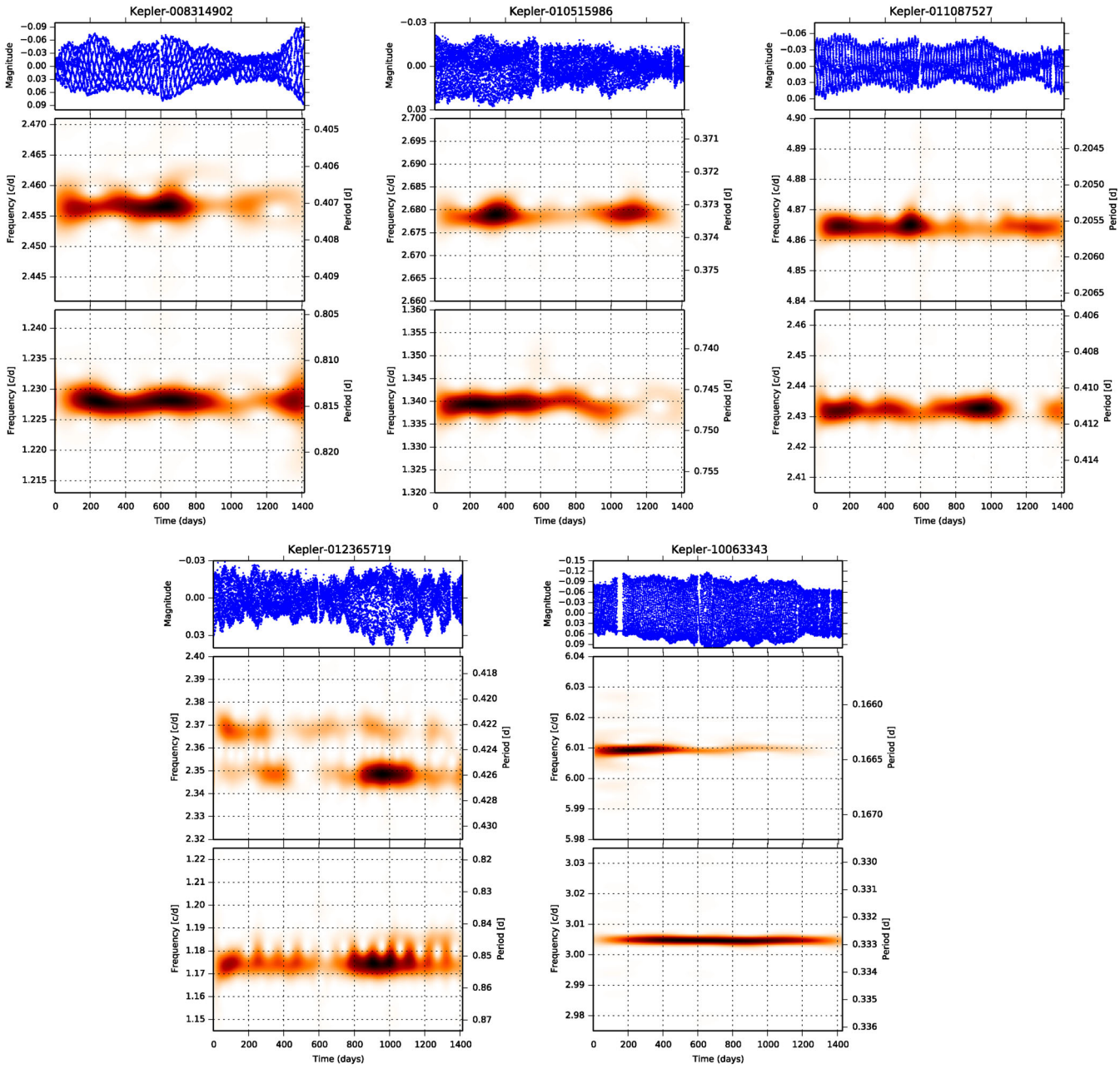

Figure 2 – *continued*

spectrum, signalling the measurable change of the rotational period of the star. As the typical spot emergence latitude – the activity belt – is shifting with the butterfly diagram, the observed main rotation frequency is also changing. For the same reason, the 2*f* regions can have different structure from the region of the main frequency: if spots are separated by ≈180°, but they are at slightly different latitudes, their signal in the Fourier spectrum can be stronger than the signal at exactly the 2*f* frequency.

5 NOTES ON INDIVIDUAL OBJECTS

Kepler-03541346. The signal of the rotation changes smoothly in time; an activity cycle with a period of ≈330 d seems to exist. The cycle can be seen pronounced at the rotation frequency (*f*), and a similar trend is visible at its double (2*f*), especially between 400 and 900 Kepler-days,[6] meaning that the shape of the cycle is not symmetric.

Kepler-04819564. We find a periodicity of ≈530 d. Frequency splits can be observed in both the rotational frequency *f* and its double 2*f*, indicating two active regions present on different latitudes with slightly different rotation periods.

Kepler-04953358. A longer term variability is seen in the rotation frequency, and its double frequency runs parallel with a period

[6] Starting at JD 245 4833.0.

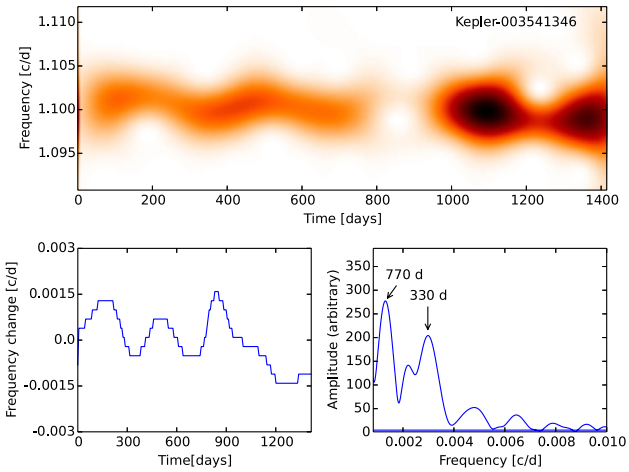

Figure 3. Top: STFT of the Kepler-003541346 light curve; bottom left: detected frequency change in the STFT; bottom right: Fourier transform of this change with a (probably fake) signal at 770 d and a real signal at 330 d.

of ≈600 d. The long-term variation dominates the time–frequency plot, but to confirm its existence, a longer data set is needed.

Kepler-05791720. We find a periodicity of ≈320 d, which is present in both the *f* and 2*f* frequencies. The light curve shows very frequent flare activity which is seen in Fig. 2 as deviating brighter data points.

Kepler-06675318. A hint for a periodicity of ≈370 d can be seen. The 2*f* plot indicates a periodicity of similar value.

Kepler-07592990. There is a sign for an ≈500-d-long variation in the rotation frequency. Besides the rotation signal, the Fourier spectrum shows another period around 20 d. According to DSS[7] images, there is a close-by source to this target. Thus, we examined the target pixel file from Q12, to find out the origin of this signal. We checked Fourier transforms of light curves from different pixels and pixel sets. According to this analysis, this longer, 20-d-long period is most possibly associated with the contaminating source. Unfortunately, the two objects are too close to each other to create a contamination-free aperture. We checked the STFT analysis after prewhitening the light curve with the 20-d-long period; there was no change in the result.

Kepler-08314902. In the region of the rotation frequency, a variation with a period of ≈610 d is seen. The region of the double frequency shows a clear variation of ≈330 d, and a period of ≈470 d can also be seen. These double signals might be a result of multiple cycles, but a longer data set is needed to confirm.

Kepler-10515986. Certainly there is a variation in the rotational period, but no typical cycle length can be easily given; the first 500 d show quite irregular behaviour. Our best estimation is 300–400 d. The light curve shows frequent flares.

Kepler-11087527. The *f* region suggests periodicities of ≈310 and ≈650 d, which are also present in the 2*f* region.

Kepler-12365719. Two distinct frequencies can be seen on this target, and there is a variation of in the rotational frequency with a time-scale of a few hundred days. The two nearby frequencies do not allow us to determine a more precise value. We examined both DSS images and the *Kepler* Full Frame Images, but no visible close-by stars could be seen. Since the pixel size of the *Kepler* CCD is 4 arcsec, a contaminating source cannot be safely ruled out by visual inspection of the images. Another interesting possibility could be that this target is a close binary system with components having slightly different rotational periods, similar to BY Dra (Pettersen, Oláh & Sandmann 1992). If this is a single target, that would mean that two very persistent active nests are present on the object, at two distinct latitudes during the full length of the observations which do not move, and no (or undetectable) other active region appears. We consider this last scenario less likely.

[7] Digitized Sky Survey, available at http://aladin.u-strasbg.fr/

6 DISCUSSION

McQuillan et al. (2013a) studied the rotation of about 2500 *Kepler* M dwarfs with a method based on autocorrelation. Their sample with detected rotation contains four of our cycling targets: KIC 4953358, KIC 5791720, KIC 10515986 and KIC 12365719. In all cases, their rotation periods derived by an independent method show very good agreement with our values.

6.1 Estimation of the differential rotation shear

We estimate the α parameter, which is often used in practice to describe the shear of the differential rotation, and is defined as $\alpha = \Delta\Omega/\Omega_{\rm eq} = (\Omega_{\rm eq} - \Omega_{\rm pole})/\Omega_{\rm eq}$. If we suppose that the extrema of the rotation periods ($P_{\rm rot,\,min}$, $P_{\rm rot,\,max}$) we found represent the rotation at the equator and the pole, we can give a lowest estimation of the α parameter using the $P_{\rm rot}$ and $\Delta P_{\rm rot}$ for each object – these values are summarized in Table 1. Note that by using this method, it is not possible to determine if the differential rotation is solar or anti-solar, since we have no latitude information from where the rotational signal originates.

It is possible that the actual $P_{\rm rot}$ values span a wider range than we estimate from the extreme positions of the rotation frequency in the STFT diagram – this can be revealed by detailed Fourier analysis of segmented light curves for each target, but that is outside the scope of the current paper. This would yield higher values of α. A similar method was used by Reinhold et al. (2013) to study rotation and differential rotation in more than 40 000 active *Kepler* targets. The authors used Lomb–Scargle periodograms to find the extrema of the rotation periods during one quarter (Q3). Their sample contains seven targets from this paper,[8] and in two cases they also detected sign of differential rotation: indeed, they found higher values of α, whereas their main rotation periods for the matching targets agree with our values. In the case of KIC 3541346 and KIC 4953358, they found $\alpha = 0.0101$ and 0.0123, respectively. The authors did not (and could not) take into account that the active regions might emerge only in a smaller latitude range; thus, the differential rotation shear could be even higher. Given the nature of the method, the uncertainty in the spot latitudes does not allow accurate determination of the shear. Note that the authors used an oversampling of 20 that might result in peaks that are not real and could change the values of α they found.

To give a better estimate, we should know the actual latitude values where the active regions emerge during the cycle, for which we can give only crude guesses. By assuming the usual quadratic differential rotation law of

$$\Omega(\vartheta) = \Omega_{\rm eq}(1 - \alpha \sin^2 \vartheta), \quad (1)$$

[8] KIC 03541346, KIC 04953358, KIC 05791720, KIC 06675318, KIC 08314902, KIC 10515986 and KIC 12365719.

the shear can be determined from known rotation periods at given latitudes using the following equation:

$$\alpha = \frac{\Omega(\vartheta_2) - \Omega(\vartheta_1)}{\Omega(\vartheta_2)\sin^2\vartheta_1 - \Omega(\vartheta_1)\sin^2\vartheta_2}. \quad (2)$$

If we assume latitudes similar to the solar case, where the spots emerge between 0° and 30° latitudes, the given α values are higher by a factor of ≈4; however, this scenario is unlikely (see e.g. Işık et al. 2011). In a case based on the fast-rotating ($P_{\rm rot} = 2$ d) K0 dwarf model of Işık et al. (2011), where the spots emerge between ≈35° and ≈45° latitudes (cf. fig. 10 of that paper), the α values in Table 1 get higher by a factor of ≈6 and we get a typical value of $\alpha = 0.010$ for our sample.

For a more realistic estimate, a dynamo model for fast-rotating late-type dwarfs is needed that can more accurately predict the emergence latitudes. Brown et al. (2011a) studied magnetohydrodynamic models of a fast-rotating Sun and found wreath-like magnetic structures in the convection zone around 5–25° latitudes. Işık et al. (2011) presented models of solar-like and main-sequence K-type stars of different rotation rates, but a model of ultrafast-rotating late-type stars is a real challenge for the theoreticians. Another way of getting more accurate values for α would be to determine directly the active region latitudes from the light curves by analytic modelling or inversion of the light curves. However, the information on the actual latitudes is very limited in photometric data, and is present only in the limb darkening of the spotted surface.

6.2 Rotation–cycle length relation

In Oláh et al. (2009), a new correlation between the cycle length normalized with the rotation and the inverse rotation period is given in log–log scale, with one single M dwarf star in the sample (EY Dra) with a quite short cycle period, which was not used in determining the slope of the relation. Vida et al. (2013) find that the activity cycles for ultrafast-rotating dwarfs are somewhat shorter than the previous samples would indicate, by extending the relation based on stars of slower rotation. In that work, another M dwarf, V405 And, a binary, was added to the stars with known cycles.

Using the activity cycles from Oláh et al. (2009) and Vida et al. (2013), and adding the results of the present paper, we studied again the rotation–cycle length relation (see Fig. 4). Two stars from the present sample seem to have double cycles, but the longer ones are uncertain due to the limited length of the data set; thus, only the shortest cycles have been considered. Savanov (2012), using data from the All Sky Automated Survey (ASAS) for a homogeneous set of only M dwarf stars, did not find any relation between the lengths of rotations and cycles. Looking at Fig. 4 we find that four stars with certain cycles derived in the present paper, and two stars from Vida et al. (2013), V405 And and EY Dra (which are M dwarfs), fit well the M dwarf sequence by Savanov (2012), except one star, KIC 04819564. We thus excluded the M dwarf stars from the fits of Fig. 4 but included KIC 04819564. The slope for all the cycles and for the shortest cycles (in the case of multiple cycles) is 0.77 ± 0.06 and 0.78 ± 0.05, similarly to the earlier values of 0.74 by Baliunas et al. (1996) and to 0.81 for all the data and 0.84 for the shortest cycles by Oláh et al. (2009).

The existence of a relation between the cycle lengths and rotational periods for a diverse sample of active stars (the sample contains both single and binary stars, giants and dwarfs, of different spectral types) did not change with the exclusion of the M dwarf stars. Already the short-period part ($P_{\rm rot} < 1$ d) of cycling stars seems to separate by spectral type, and was not evident in Vida et al. (2013) which was prepared before the results of Savanov (2012) were published, without the table cycle lengths.

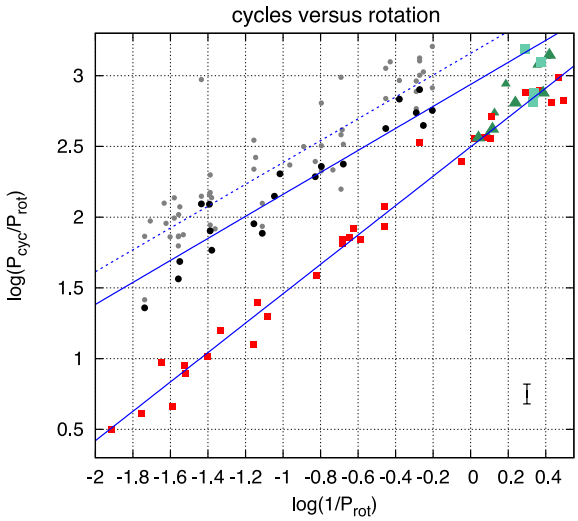

Figure 4. Correlation between the rotation period and the length of the activity cycle, as in Oláh et al. (2009). Large black dots, green squares and green triangles stand for the shortest cycles from Oláh et al. (2009), results from Vida et al. (2013) and those from the present paper, respectively. Smaller grey dots denote data from different surveys, from Oláh et al. (2009). Smaller triangles mark the less certain periods from this paper (marked with ‡ in Table 1). Red filled squares show data for M dwarf stars from Savanov (2012). The dotted line represents the fit to all the data from Oláh et al. (2009), Vida et al. (2013) plus the results of the present paper excluding M stars, while the parallel line shows the fit to the shortest cycles of that data set. The slope of the fit to the data from Savanov (2012) is close to 1.0, which means that no correlation is found between rotation and cycle lengths. Error bars on the lower right indicate the typical uncertainty of rotation period and activity cycle determination (error bar of the *x*-axis is smaller than the line itself). See the text for more.

The relation between rotational and cycle periods is extremely important for understanding stellar dynamos (see e.g. Baliunas et al. 1996; Brun, Miesch & Toomre 2004; Brown et al. 2011a; Augustson, Brun & Toomre 2013 for the details). The results presented in this paper, which populate the short-period end of the rotation–cycle length relation, give a good impact to this study, showing a clear separation between the K and M dwarfs already at very short rotational periods. The determination of the exact spectral types of cycling stars studied in this work is the subject of a forthcoming paper.

7 SUMMARY

(i) We analysed light curves of 39 fast-rotating ($P_{\rm rot} \lesssim 1$ d) active stars from the *Kepler* data base using time–frequency analysis.

(ii) From the STFTs of the light curves in the region of the rotation frequency and its double, we detected quasi-periodic variations.

(iii) We interpret these variations as a result of stellar butterfly diagram: during the activity cycle the typical latitude of the starspots changes, and this, because of the differential rotation of the surface, results in change of the rotation period.

(iv) With our technique, we found hints of activity cycles with periods in the range of 300–900 d in nine targets.

(v) To find activity cycles through rotational period variation due to differential rotation and the butterfly diagram is a new method

which does not need latitudinal information as input, applicable only for very high precision and (nearly) continuous data sets such as is produced by the *Kepler* satellite.

(vi) This result populates the short-period part of the rotation–cycle length relation showing a clear separation between the K and M dwarf stars with the shortest periods ($P_{\rm rot} < 1$ d); this is very important in understanding the nature of the cycling dynamos.

ACKNOWLEDGEMENTS

We would like to acknowledge the helpful comments of the anonymous referee, which improved this paper considerably. We thank Gy. Szabó for the help with *Kepler* data and M. Váradi for his suggestions with the period analysis. We are grateful to I. Savanov for the table of M-dwarf cycles. We would also like to thank the anonymous referee for the helpful comments, which improved the paper significantly. The financial support of the OTKA grants K-81421, K-109276, K-83790, the KTIA URKUT_10-1-2011-0019 grant, and the European Community's Seventh Framework Programme (FP7/2007-2013) under grant agreements no. 269194 (IRSES/ASK) and no. 312844 (SPACEINN) is acknowledged. This work was also supported by the 'Lendület-2009', and 'Lendület-2012' Young Researchers' Programs of the Hungarian Academy of Sciences, and by the HUMAN MB08C 81013 grant of the MAG Zrt. RSz was supported by the János Bolyai Research Scholarship of the Hungarian Academy of Sciences. Data presented in this paper were obtained from the Mikulski Archive for Space Telescopes (MAST). STScI is operated by the Association of Universities for Research in Astronomy, Inc., under NASA contract NAS5-26555. Support for MAST for non-HST data is provided by the NASA Office of Space Science via grant NNX13AC07G and by other grants and contracts. Funding for the *Kepler* mission is provided by NASA's Science Mission Directorate.

REFERENCES

Augustson K. C., Brun A. S., Toomre J., 2013, ApJ, 777, 153
Baliunas S. L., Nesme-Ribes E., Sokoloff D., Soon W. H., 1996, ApJ, 460, 848
Berdyugina S. V., Henry G. W., 2007, ApJ, 659, L157
Brown B. P., Miesch M. S., Browning M. K., Brun A. S., Toomre J., 2011a, ApJ, 731, 69
Brown T. M., Latham D. W., Everett M. E., Esquerdo G. A., 2011b, AJ, 142, 112B
Brun A. S., Miesch M. S., Toomre J., 2004, ApJ, 614, 1073
Csubry Z., Kolláth Z., 2006, in Sterken C., Aerts C., eds, ASP Conf. Ser. Vol. 349, Astrophysics of Variable Stars. Astron. Soc. Pac., San Francisco, p. 215
Deeg H. J., Alonso R., Belmonte J. A., Alsubai K., Horne K., Doyle L., 2004, PASP, 116, 985
Ivezić Ž. et al., 2008, LSST: From Science Drivers to Reference Design and Anticipated Data Products, available at: http://lsst.org/lsst/overview/
Işık E., Schmitt D., Schüssler M., 2011, A&A, 528, A135
Karoff C. et al., 2013, MNRAS, 433, 3227
Katsova M. M., Livshits M. A., Soon W., Baliunas S. L., Sokoloff D. D., 2010, New Astron., 15, 274
Kolláth Z., 1990, Konkoly Observatory Occasional Technical Notes, 1, 1
Kolláth Z., Oláh K., 2009, A&A, 501, 695
Mathur S. et al., 2014, A&A, 562, 124M
McQuillan A., Aigrain S., Mazeh T., 2013a, MNRAS, 432, 1203
McQuillan A., Mazeh T., Aigrain S., 2013b, ApJ, 775, L11
Nielsen M. B., Gizon L., Schunker H., Karoff C., 2013, A&A, 557, L10
Oláh K., Strassmeier K. G., 2002, Astron. Nachr., 323, 361
Oláh K., Jurcsik J., Strassmeier K. G., 2003, A&A, 410, 685
Oláh K. et al., 2009, A&A, 501, 703
Pál A. et al., 2013, Astron. Nachr., 334, 932
Pettersen B. R., Oláh K., Sandmann W. H., 1992, Astron. Astrophys. Suppl. Ser., 96, 497
Reinhold T., Reiners A., Basri G., 2013, A&A, 560, A4
Ribárik G., Oláh K., Strassmeier K. G., 2003, Astron. Nachr., 324, 202
Savanov I. S., 2012, Astron. Rep., 56, 716
Scargle J. D., Keil S. L., Worden S. P., 2013, ApJ, 771, 33
Strassmeier K. G., Boyd L. J., Epand D. H., Granzer T., 1997, PASP, 109, 697
Strassmeier K. G., Carroll T. A., Weber M., Granzer T., Bartus J., Oláh K., Rice J. B., 2011, A&A, 535, A98
Vida K., Kriskovics L., Oláh K., 2013, Astron. Nachr., 334, 972
Walkowicz L. M., Basri G. S., 2013, MNRAS, 436, 1883
Wilson O. C., 1968, ApJ, 153, 221

APPENDIX A: TESTING THE STFT TO FIND BUTTERFLY DIAGRAMS ON SOLAR AND ARTIFICIAL DATA

To test our method, we applied it to solar observations and artificial light curves. To study the Sun in a similar way to the stars, we need disc-integrated observations, e.g. the 10 cm radio flux. The result of the STFT analysis is shown in Fig. A1 on the time-scale of decades, and also for one activity cycle. Unfortunately for the analysis, the spottedness of the Sun is low. Therefore, the changes in the typical rotation frequency are not seen well, although faster rotation is observed when the spots are closer to the equator, in the activity maximum (see the zoomed-in plot of Fig. A1), near 28 d. Note that by using the 10 cm solar flux, we are analysing large coronal structures of the Sun; therefore, the changes in the rotation frequency are not so well pronounced. A very similar time–frequency analysis was performed recently by Scargle, Keil & Worden (2013) using solar Ca II K data. They used a renormalized plot (see fig. 10 in their paper) to enhance and show the features that are otherwise lost during solar minimum – using this method, the quasi-periodic changes through the cycles can indeed be seen.

To evade problems emerging from the low spottedness of the Sun, we tested the method also on artificial data. We used a three-spot model of a fast-rotating star ($P_{\rm rot} = 0.5$ d) with an inclination of $i = 50^\circ$ produced by SpotModeL (Ribárik, Oláh & Strassmeier 2003). During the supposed 300-d-long activity cycle in the data, typical spot latitudes were changing between 30° and 70° (to simulate the higher spot latitudes due to Coriolis effect caused by fast rotation). Spot longitudes were chosen randomly and varied according to solar-like differential rotation with $\alpha = 0.01$. When generating the light curves, a small amount of random variation was added to each spot parameter. Note that the actual values of the rotation period and cycle length are completely arbitrary in this simulation; they affect only the time-scale of the variations, but were chosen to be similar to the values we found in the *Kepler* stars. We plotted two examples of the results using STFT analysis on these artificial data in Fig. A2 and A3. Spot coverage variation was set between 3 and 10 per cent. In the first case, our analysis gave a cycle length of 301 ± 40 d, while in the second case the result was 300 ± 35 d. In both cases, the supposed 300-d-long cycle length was recovered correctly.

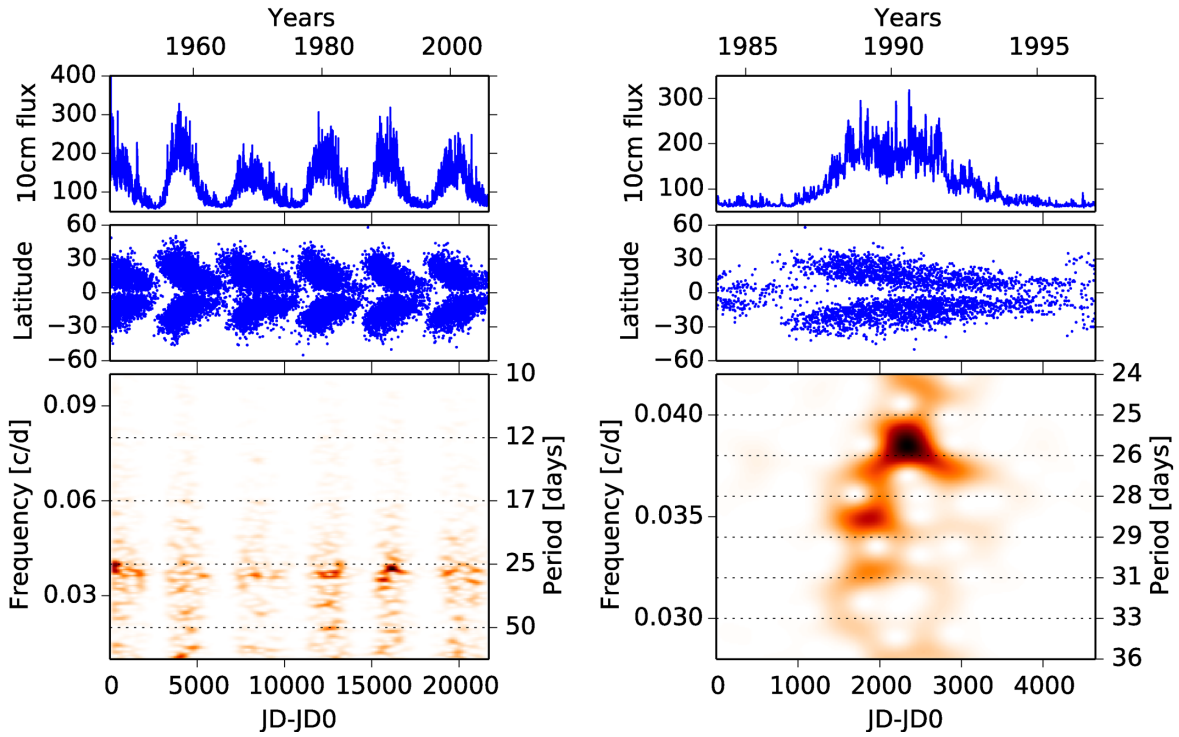

Figure A1. Testing the STFT method on solar radio data. Both plots show the 10 cm radio flux (top), the butterfly diagram (time–spot latitude diagram, middle) and the result of the STFT analysis. The low spottedness of the inactive Sun does not make the possible detection of cycles very uncertain, although some changes in the detected rotation period might seem on the right zoomed-in plot.

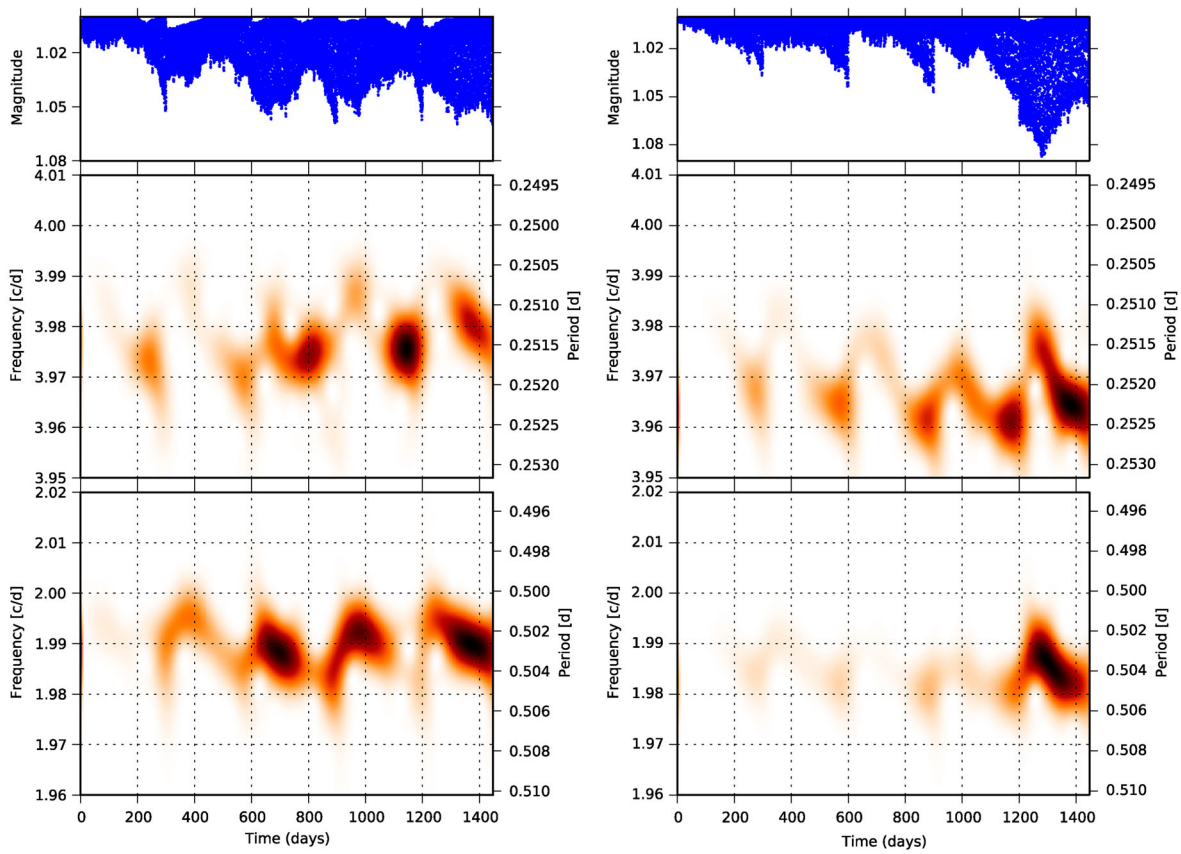

Figure A2. Testing the STFT method on artificial light curves. The cycle length could be recovered in both cases within the errors, although the large amplitude differences in the light curve and the weighting in the STFT plotted on the right make the recognizing harder.

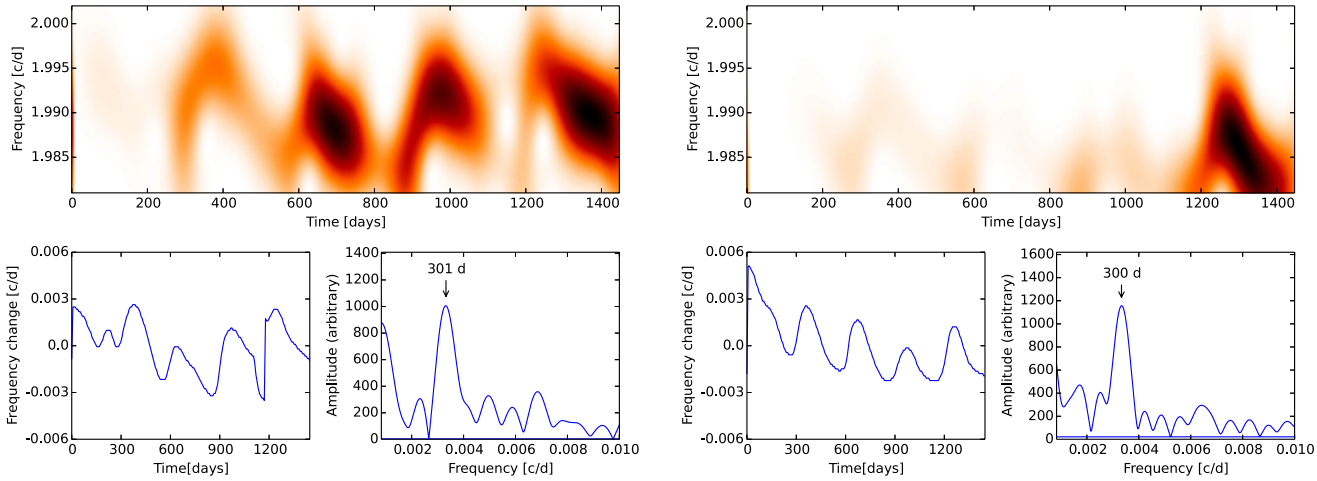

Figure A3. Recovering cycle length from artificial data. The light curves are the same as plotted in Fig. A2. The results return correctly the 300-d-long periods.

This paper has been typeset from a TEX/LATEX file prepared by the author.